*Journal of the Brazilian Computer Society, 2026, 32:1,* doi: 10.5753/jbcs.2026.7346


# Efficient and Fast Kolmogorov–Arnold Networks for Chest X-Ray Classification of Pneumonia and Tuberculosis

**Alexsander Lindolfo de Lima** [ **Federal University of Uberlandia** | ***aleder.lima@ufu.br*** ]
**Henrique Fernandes** [ **Federal University of Uberlandia** | ***henrique.fernandes@ufu.br*** ]
**Jose dos Reis V. Moura Junior** [ **Federal University of Uberlandia** | ***zereis@ufu.br*** ]

*Faculty of Computing, Federal University of Uberlandia, Uberlandia, MG, 38408-100, Brazil.*

**Received:** 02 January 2026 • **Accepted:** 02 July 2026 • **Published:** 10 July 2026

**Abstract** Interpreting chest X-ray images can be challenging, leading to an increasing reliance on computational methods by physicians to improve diagnostic accuracy and disease monitoring. Among these methods, machine learning models—particularly those in computer vision, such as Convolutional Neural Networks (CNNs)—have shown strong performance in image classification tasks. Recently, Kolmogorov-Arnold Networks (KANs) have emerged as an alternative framework that redefines how connections and activations are computed within neural architectures. This study aims to develop a classification system using a dataset of 5,000 chest X-ray images categorized as Normal, Pneumonia, or Tuberculosis. Two KAN-based algorithms, Efficient KAN (EKAN) and Fast KAN (FKAN), were implemented and compared with a CNN baseline. Experimental results show that the FKAN model achieved performance comparable to CNN with approximately 96% accuracy in test cases, but with a reduced computational cost of approximately 96.18%. The results suggest that the FKAN and EKAN algorithms are a practical and efficient approach for medical image classification.

**Keywords:** Convolutional Neural Networks, Kolmogorov-Arnold Networks, Lung diseases

## 1 Introduction

According to a 2021 publication by the World Health Organization (WHO), five of the ten leading causes of death worldwide are respiratory diseases: COVID-19, Chronic Obstructive Pulmonary Disease (COPD), Acute Lower Respiratory Infections, Cancer (Trachea, Bronchus, and Lung), and Tuberculosis (WHO [2023]). Among the various diseases affecting the respiratory system—a major challenge in the health field—pneumonia (infection of the pulmonary alveoli) and tuberculosis (infection of alveolar macrophages) are among the leading causes of death globally, as reported by the (WHO [2023]; Patel *et al*. [2024]; ul Haque *et al*. [2024]; Lai *et al*. [2024]).

Among the various methods used to diagnose lung diseases, chest X-rays stand out due to their simplicity, cost-effectiveness, and efficiency. Computed tomography (CT) is also used, producing more detailed images through higher radiation levels combined with computer processing. To interpret these images, healthcare professionals use machine learning techniques to assist in diagnosis and patient monitoring (Anthimopoulos *et al*. [2016]; Fernández-Miranda *et al*. [2024]; Hasan *et al*. [2024]; Kieu *et al*. [2018]).

Among the various machine learning techniques, those in the field of computer vision are particularly notable, such as Convolutional Neural Networks (CNNs). CNNs are based on the Universal Approximation Theorem, which states that any continuous function can be approximated provided the activation function is continuous and non-linear. This technique enables image analysis by generating new feature maps through convolutional operations (Hornik *et al*. [1989]; Jiao and Zhao [2019]; LeCun *et al*. [1998]).

On the other hand, Kolmogorov-Arnold Networks (KANs) are described by their creators as a promising alternative to traditional Artificial Neural Network (ANN) techniques. This model is based on the Kolmogorov-Arnold Representation Theorem, where any continuous, multivariate function can be represented by the sum of composite one-dimensional functions. Unlike the architecture of Artificial Neural Networks—where activation functions are fixed in artificial neurons and connections are linear—in this new approach, artificial neurons only perform summation operations, while activation functions are adjusted within the connections (Kolmogorov [1957]; Liu *et al*. [2024b]).

Therefore, the objective of this study is to develop an image classification system using CNN, Efficient KAN (EKAN) (Blealtan [2024]) and Fast KAN (FKAN) (Li [2024]) algorithms, applied to chest X-rays to assist in the diagnosis of pulmonary diseases such as Pneumonia and Tuberculosis. To the best knowledge of the authors, it is the first time FKAN and EKAN is being applied in these type images/diseases. Data augmentation techniques were employed to simulate different conditions that may occur during image capture and to prevent overfitting.

The remainder of this paper is organized as follows: Section 2 presents related work using machine learning for lung disease classification and studies utilizing the KAN architecture. Section 3 details the methodology, including dataset construction, hardware, programming language, and model implementation. Section 4 discusses the results. Finally, Section 5 presents the conclusions and a comparative analysis of the results.

# 2 Related works

Considering the vast literature in the health field focused on classification using machine learning, this section presents references where authors have used CNN models for the detection of lung diseases through X-ray images, studies involving the KAN architecture for specific problems, and KAN models for solving problems that are part of the scope of lung disease classification using X-ray images.

## 2.1 CNNs applied to X-ray images

Arias-Londoño *et al.* [2020] used a CNN architecture for the automatic detection of COVID-19 through chest X-ray images. The objective was to evaluate how image pre-processing techniques affect results and potentially compromise the system by simulating different image conditions. As a result, a precision of 91.5% and an average recall of 87.4% were achieved.

Muñoz-Aseguinolaza *et al.* [2023] utilized a CNN architecture for 3D medical image analysis to detect lung cancer, extracting relevant information from three-dimensional data. This approach achieved an accuracy of 76.44%.

Ausawalaithong *et al.* [2018] employed the DenseNet-121 model, based on CNN architecture, to identify lung cancer in chest X-rays. They achieved an average accuracy of 70%, demonstrating the effectiveness of this approach on a dataset with limited samples.

Hamal *et al.* [2024] tested various machine learning models for COVID-19 detection from chest X-rays. Notably, the VGG-19 model (based on CNN architecture) stood out, achieving a precision of 99% in training and 98% in testing—specifically 90% for COVID-19, 90% for normal cases, and 100% for pneumonia—proving the effectiveness of this approach in classifying lung diseases.

Alshmrani *et al.* [2023] also used the VGG-19 model for classifying Pneumonia, Lung Cancer, Tuberculosis, Pulmonary Opacity, and COVID-19 using chest X-rays. After image preprocessing, the proposed methodology achieved 96.48% accuracy, 93.75% recall, 97.56% precision, 95.62% F1 score, and 99.82% ROC-AUC, demonstrating high performance for effective diagnosis.

Al-Sheikh *et al.* [2023] proposed an automatic system for detecting Pneumonia and COVID-19 using chest X-rays and CT images, employing the k-symbol Lerch transcendental function model for image enhancement, a custom CNN architecture, and two pre-trained deep learning models (AlexNet and VGG-16). For the chest X-ray dataset, they achieved 98.60% accuracy, 98.40% sensitivity, and 98.50% specificity. For the CT dataset, they reached 98.80% accuracy, 98.50% sensitivity, and 98.40% specificity, highlighting the advantages of using image enhancement models in initial processing steps.

## 2.2 General implementations of the KAN

According to a systematic review on the fundamentals and applications of KAN architecture by Somvanshi *et al.* [2024], significant algorithmic advancements include Temporal-KAN (Xu *et al.* [2024b]), Fast KAN (Li [2024]), and Partial Differential Equation-KAN. These models have shown improvements and adaptations for solving complex problems. Furthermore, KAN can be integrated with CNN (Abd Elaziz *et al.* [2024]; Bodner *et al.* [2024]; Igali and Shamoi [2024]; Drokin [2024]), RNN (Genet and Inzirillo [2024]) and Transformers (Xie *et al.* [2024]), due to its versatility in hybrid architectures.

Liu *et al.* [2024a] mention that several studies have aimed to develop KAN applications in other fields. Concluding remarks highlight the effectiveness of this technique compared to traditional ANNs in areas such as graph learning (Kiamari *et al.* [2024]; Bresson *et al.* [2024]; De Carlo *et al.* [2024]), computer vision (Cheon [2024]; Firsov *et al.* [2024]), time series analysis (Vaca-Rubio *et al.* [2024]), and usage with other one-dimensional functions like Wavelet (Bozorgasl and Chen [2024]), Fourier (Xu *et al.* [2024a]) and Jacobi (Aghaei [2025]).

## 2.3 KANs applied to X-ray images

Qezelbash-Chamak *et al.* [2025] presented KANBalance, a framework developed to mitigate class imbalance in medical images by combining Kolmogorov-Arnold Networks with the Focal Loss cost function, which focuses learning on correcting difficult-to-classify examples. Validated on imbalanced datasets, KANBalance outperformed traditional resampling techniques such as SMOTE and ADASYN, achieving 96.22% accuracy in detecting pneumonia in pediatric X-rays and 96.05% accuracy in identifying brain tumors.

Fatema *et al.* [2025] focused on clinical environments with scarce data and limited computational resources, introducing three KAN models: SBTAYLOR-KAN (B-splines with Taylor series), SBRBF-KAN (B-splines with Radial Basis Functions), and SBWAVELET-KAN (B-splines within Morlet wavelet transforms). The SBTAYLOR-KAN model achieved the best performance when processing raw medical images, reaching a maximum accuracy of 98.93% in tuberculosis X-rays and 86% accuracy using 30% of the original training data. The main difference highlighted by the authors lies in its structural efficiency, since the model achieved these results using 2872 trainable parameters, which represents a reduction in computational cost compared to traditional convolutional architectures that require millions of parameters.

Pan and Wang [2026] proposed MedVK, integrating Kolmogorov-Arnold Networks with Transformers to decouple spatial and channel modeling. The model was evaluated on various datasets, such as chest X-ray images (PneumoniaMNIST and CPN X-ray). The results showed that MedVK outperformed traditional architectures such as ResNet50 and MedViTV2, achieving better overall accuracy and AUC in the classification of these images, requiring up to 20 times less processing (GFLOPs).

He *et al.* [2026] developed the VKT hybrid model, which combines local extraction via parallel KAN operations (ConvKan) with a Local-Global Attention (LG) branch. In tests conducted on seven datasets, including the use of X-ray images for COVID-19 and pneumonia diagnosis (CPN X-Ray), VKT outperformed state-of-the-art models with accuracy gains of 0.2% to 4.1%. The architecture proved highly accurate for X-ray analysis, operating efficiently with only 14.16

million parameters.

Wang *et al*. [2025] introduced MedKAFormer, which incorporates the Kolmogorov-Arnold theorem into the ViT stages to mitigate the high parameter cost. The model was tested on 14 datasets, such as chest X-ray image sets (CPN X-ray and PneumoniaMNIST). The results demonstrated a reduction in parameters (85.61% compared to ViT-Base), while the representation quality was improved, evidenced by a notable 6.2% increase in the AUC metric specifically in the CPN X-ray dataset.

Yang *et al*. [2025] presented MedKAN, replacing fixed activation functions with learnable nonlinear transformations (RBFs) in two extraction fronts: local and global. The model validation encompassed nine sets of medical images, including the analysis of pediatric chest X-ray images (PneumoniaMNIST). The results demonstrated that the model maintained high efficiency, with the MedKAN-B variant achieving high accuracy in radiographs compared to CNN and Transformer models of equivalent size.

Riechie *et al*. [2025] evaluated the Convolutional Kolmogorov-Arnold Network (CKAN) model for pneumonia detection, focusing on the analysis of pediatric chest X-ray images. The architecture extends the principles of KAN networks to the convolutional domain, replacing fixed weights with learnable nonlinear spline-based functions, which improves the ability to capture complex relationships in radiographs. The results demonstrated that the proposed model outperformed baseline CNN networks: the best-performing variant (CKAN Medium) achieved an accuracy of 83.49%, precision of 79.96%, and recall of 98.21% in detecting the disease via X-ray, compared to 81.00% accuracy for the best CNN. In addition to demonstrating superior performance in disease screening, the CKAN architecture showed better generalization capabilities and proved to be more robust in handling data imbalances, significantly minimizing false negatives for diagnosis.

Although the reported works have used Transformers in their respective scopes, this being one of the most widely used techniques today, there is a need for experimentation with simple and customized models based on the KAN architecture, not only due to the lack of articles in the literature, but also in contexts of scarce computational resources.

# 3 Methodology

This section presents the theoretical foundation of the KAN architecture, as well as the Efficient KAN and Fast KAN algorithms proposed by Blealtan [2024] and Li [2024], respectively. Subsequently, the dataset creation and the implementation methodology for these algorithms are described.

## 3.1 Kolmogorov-Arnold networks

As mentioned in Section 1, the core calculation for the KAN architecture involves summing one-dimensional composite functions, as shown in Equation 1 (Liu *et al*. [2024b]).

$$f(x_1,\ ...,\ x_n) = \sum_{q=1}^{2n+1} \Phi_q \left( \sum_{p=1}^{n} \phi_{q,p}(x_p) \right), \qquad (1)$$

where $x$ represents the input variables, $n$ is the number of variables, $f$ is the continuous multivariable function, $p$ represents the input dimensions, and $q$ corresponds to the output dimensions. The one-dimensional continuous functions depending on a single variable are represented by $\Phi$ and $\phi$, as shown in Equation 2 (Liu *et al*. [2024b]).

$$\phi(x) = w(b(x) + spline(x)), \qquad (2)$$

where $b$ is the base function (such as SiLU and ReLU), $w$ is a factor controlling the magnitude of the activation function (initialized via Xavier initialization), and $spline$ (initialized with values close to zero) is a linear combination of B-splines, as shown in Equation 3 (Liu *et al*. [2024b]; Gordon and Riesenfeld [1974]).

$$spline(x) = \sum_i c_i B_i(x), \qquad (3)$$

where, $c$ is the adjustable vector and $B$ is the B-spline function. Using the recursive de Boor-Cox algorithm, the function is calculated as follows, that, using the recursive DeBoor-Cox algorithm, Equation 4 is calculated (Liu *et al*. [2024b]; Gordon and Riesenfeld [1974]).

$$\begin{aligned} B_{i,m}(x) = \frac{s - x_i}{x_{i+m-1} - x_i} . B_{i,m-1}(s) \\ + \frac{x_{i+m} - s}{x_{i+m} - x_{i+1}} . B_{i+1,m-1}(s)^*, \end{aligned} \qquad (4)$$

where $x_i$ is the element of the node vector, $s$ is the evaluation point, and $m$ is the order of the B-spline, which can be constant, linear, quadratic, or cubic (Gordon and Riesenfeld [1974]).

## 3.2 Efficient KAN Algorithm

Blealtan [2024] proposed adaptations to improve efficiency without sacrificing functionality. A primary issue with the KAN architecture was memory consumption related to expanding the input tensor to the format (batch_size, out_features, in_features) for activation function application. To resolve this, the input is activated by B-spline functions first, followed by linear combinations of these activations. Previously, all linear combinations were performed before calculating the B-spline functions. Another adaptation was replacing L1 regularization on input samples with regularization applied to the weights.

## 3.3 Fast KAN Algorithm

Li [2024] used the Efficient KAN algorithm as a basis to develop the FAST KAN algorithm, where the main differences lie in the replacement of the B-spline weight activation function with a radial basis function (RBF) using a Gaussian kernel and in normalization operations between the linear layers. These adaptations aimed to speed up the model, since each function is centered at different points in the input space, as shown in Equation 5.

$$f(x) = \sum_{i=1}^{N} w_i \phi(||x - c_i||), \tag{5}$$

where, $N$ is the total number of centers, $w$ are the adjustable coefficients, $x$ represents the input data, $c$ is the center, and $\phi$ is the Gaussian kernel, as shown in equation 6 (Li [2024]).

$$\phi(r) = exp\left(-\frac{r^2}{2h^2}\right), \tag{6}$$

where, $h$ controls the width/dispersion of the function and $r$ is the radial distance (Li [2024]).

## 3.4 Dataset description

A dataset containing 5000 images was used, divided into three classes: Normal (1,667 images), Pneumonia (1,667 images), and Tuberculosis (1,666 images) (de Lima [2024]).

The dataset was aggregated from four different sources to ensure classes do not overlap, preventing overfitting (Kermany *et al*. [2018]; Rahman *et al*. [2020]; Kiran and Jabeen [2024]; Chauhan *et al*. [2014]). Figure 1, Figure 2, and Figure 3 show examples of images representing Normal, Pneumonia, and Tuberculosis classes, respectively.

**Figure 1.** Normal X-ray (Rahman *et al*. [2020]).

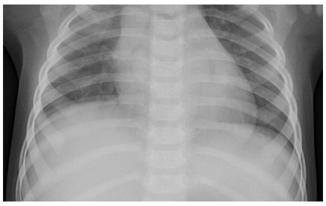

**Figure 2.** Pneumonia X-ray (Kermany *et al*. [2018]).


**Figure 3.** Tuberculosis X-ray (Kermany *et al*. [2018]).

## 3.5 Materials and implementations

All implementations were performed in Python using the PyTorch library as a basis for model development. Three different machines were used, one for each model, and their specifications can be seen in Table 1.

**Table 1.** Hardware used.

| Model | CPU | GPU | RAM |
|---|---|---|---|
| CNN | Ryzen 5 5600 | RTX 3060 12GB | 62GB |
| EKAN | Ryzen 5 5500 | RTX 2060 6GB | 31GB |
| FKAN | i5 3470 | GTX 1650 4GB | 16 GB |

For data augmentation, the torchvision library's transforms module was used with the following functions, based on the work of Baltruschat *et al*. [2019]; Chokchaithanakul *et al*. [2022]; Arsomngern *et al*. [2019]:

- Standardization of dimensions to 164x164;
- Random rotation of 10 degrees;
- Random image shifting up to 10% of its size, both horizontally and vertically;
- Random scaling between 90% reduction and 110% increase of the images relative to their size;
- Random shear adjustment of $\pm 10$ degrees;
- Random brightness adjustment in a range of $\pm 20\%$;
- Random contrast adjustment in a range of $\pm 20\%$;
- Random color intensity adjustment in a range of $\pm 10\%$;
- Random hue adjustment in a range of $\pm 10\%$.

Data augmentation techniques were applied to the images after implementing 10-fold cross-validation using the scikit-learn library, where images were randomly distributed with reproducibility enabled. In this experimental protocol, no data leakage or artificial performance due to overfitting situations occurred. Standardized parameters for all models included: mini batches = 16, epochs = 200, learning rate = 0.001, random state = 42, optimizer = ADAM, loss function = Cross-entropy, activation function = ReLU, and output function = Softmax.

The CNN algorithm was implemented using PyTorch's Sequential module shown in Figure 4, where the resizing operation was implemented to ensure that the number of pixels is reduced by half using the following parameters: Kernel size = 2, Stride = 2, and Padding = 0. The convolutional layers were implemented using the following parameters: kernel size = 3, stride = 1, and padding = 1.

The EKAN and FKAN algorithms were implemented using the KAN() framework from the efficient_kan, with the number of grid intervals = 5 and order of the polynomial = 3, and fastkan, with the number of centers = 8, libraries. Table 2 presents the architecture used.

**Table 2.** Network architecture of the EKAN and FKAN modules.

| Layer | Description |
|---|---|
| Input layer | 80688 artificial neurons |
| Hidden layer 1 | 164 artificial neurons |
| Hidden layer 2 | 64 artificial neurons |
| Hidden layer 3 | 32 artificial neurons |
| Output layer | 3 artificial neurons |

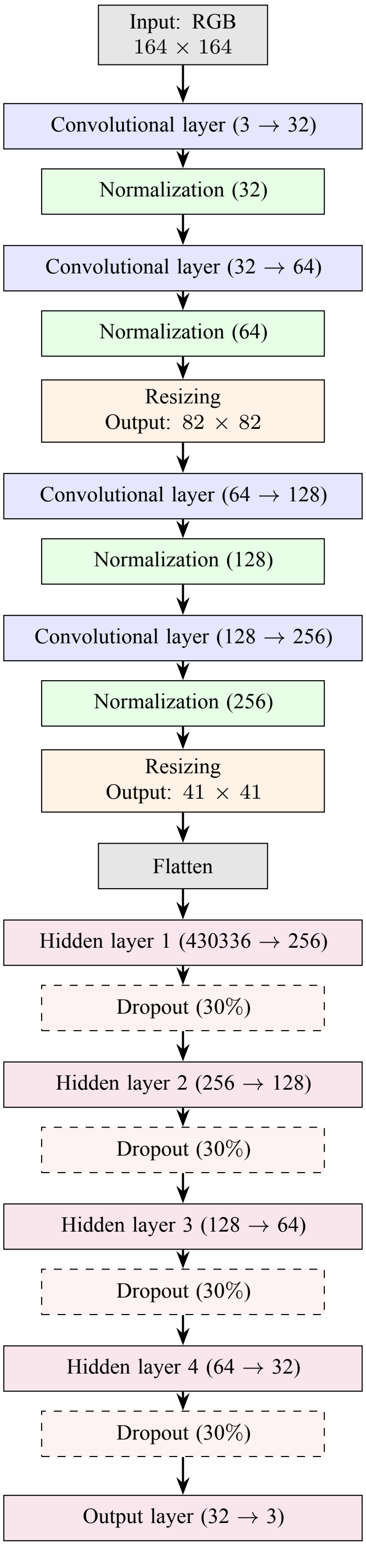


**Figure 4.** CNN architecture diagram.

# 4 Results

Following the training phase using 10-fold cross-validation, the performance of CNN, EKAN, and FKAN models was quantitatively assessed. The analysis focuses on three main aspects: convergence stability, classification metrics, and computational efficiency. Figure 5 illustrates the loss values across the 10 folds for training, while Figure 6, Figure 7, and Figure 8 present the boxplot distributions for Accuracy, Precision, Recall, and F1 Score.

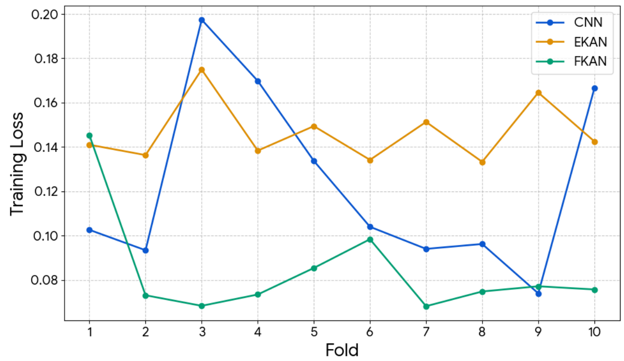


**Figure 5.** Loss values of training across folds.

## 4.1 Convergence and Stability Analysis

As demonstrated in Figure 5, the FKAN model exhibited superior convergence stability compared to the baseline models. The loss variation for FKAN remained from the range (0.0681 - 0.1452) with an average of 0.0839 and standard deviation of 2.21%, indicating a robust optimization path that is less sensitive to data initialization. In contrast, the CNN model showed significant instability, with loss values fluctuating between 0.0739 and 0.1974 with an average of 0.1231 and standard deviation of 3.92%. This high variance suggests that the CNN is more prone to local minima or overfitting depending on the specific data fold, making it less reliable for clinical deployment without extensive tuning. The EKAN model showed good stability (loss of approximately 0.1332 to 0.1749) and standard deviation of 1.3%, with consistently better performance than CNN, and better convergence accuracy than FKAN. However, although it is the most stable, its average loss (0.1465) ended up being the highest of the three models (compared to 0.0839 for FKAN and 0.1231 for CNN).

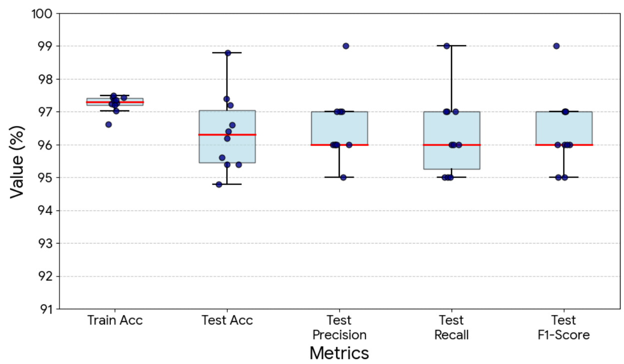


**Figure 6.** CNN Boxplot distribution.

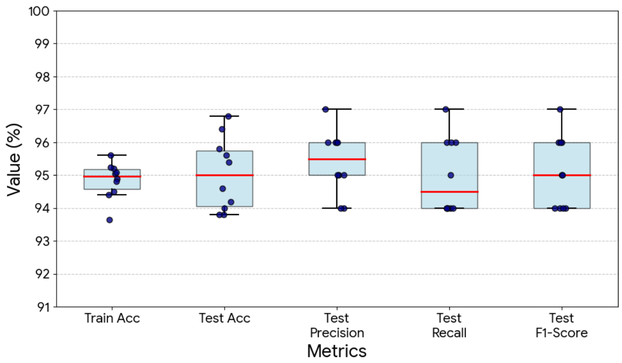


**Figure 7.** EKAN Boxplot distribution.

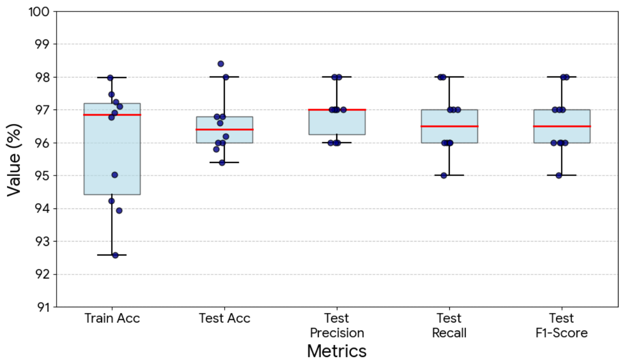


**Figure 8.** FKAN Boxplot distribution.

## 4.2 Classification Performance

Overall, all three models perform above 95% accuracy, with the FKAN algorithm matching the average accuracy of the CNN algorithm at 96%, but they have different profiles in how they handle each type of image.

The CNN model presented the highest overall average accuracy, at 96.60%. Despite fluctuating more during training, as seen in Figure 5, this model delivered the highest raw accuracy rate during cross-validation.

The FKAN model was statistically tied with the CNN, with average accuracy in 96.38%, demonstrating excellent generalization ability, with the benefit of having a lower and more stable training loss, as seen in Figure 5.

The EKAN model had a slightly lower overall performance than the other two, at 95.04%, which is consistent with the fact that it showed the greatest average loss during training.

Regarding performance by class, the three models show a consistent pattern of behavior: Tuberculosis is the most easily detected category, achieving F1 scores between 97% and 98% and 99.7% accuracy in the CNN model. The main challenge lies between the Normal and Pneumonia classes, where the models demonstrate an excellent ability to detect normal cases, with recall between 98% and 99%, but with reduced accuracy, between 89% and 93%, indicating a tendency to generate false positives by classifying slightly anomalous images as healthy. Conversely, when the networks classify an image as Pneumonia, the accuracy is 97% to 98%, but the recall is the lowest of the set, at 90% to 93%, revealing that the architectures end up committing false negatives by not detecting some infections. In this scenario, FKAN stands out as the most balanced option to minimize these errors, while CNN excels in raw accuracy, and EKAN follows the same trend with slightly lower metrics. Figures 9, 10, and 11 present the average confusion matrices for the FKAN, CNN, and EKAN models, illustrating what has been described.

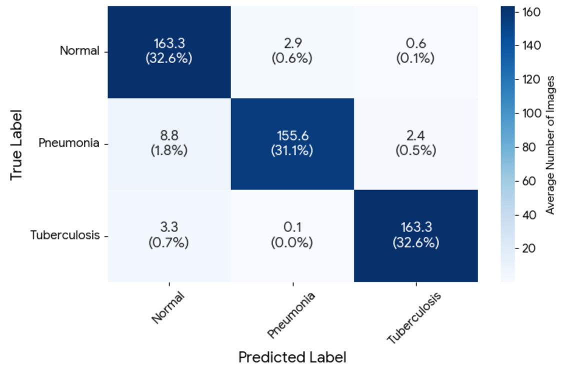


**Figure 9.** FKAN Confusion matrix.

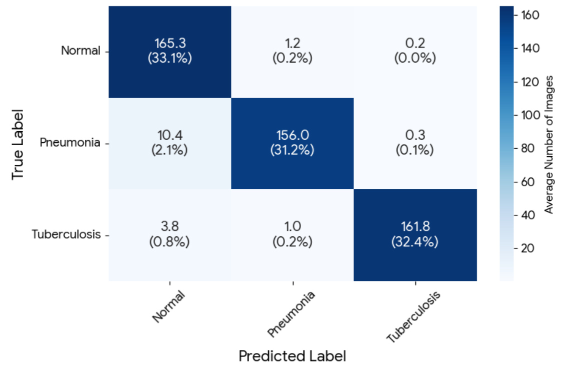


**Figure 10.** CNN Confusion matrix.

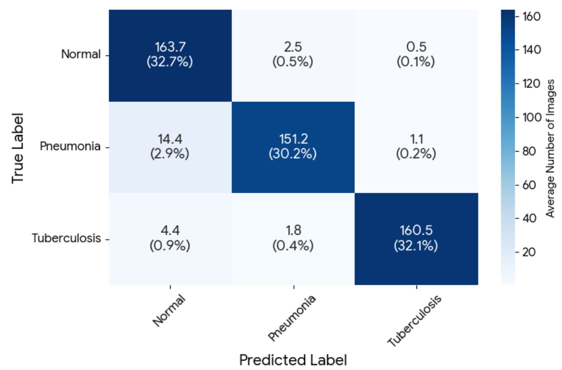


**Figure 11.** EKAN Confusion matrix.

## 4.3 Computational Cost

A comparative analysis of memory consumption reveals a significant advantage for KAN-based models. As detailed in Table 3, FKAN model stands out as the best overall choice, as it maintains accuracy in the 96% range (almost identical to CNN) with a reduction of more than 26x in computational cost.

## 4.4 Future Directions

Given these promising results, future work should focus on further validating the KAN architecture, including testing

**Table 3.** Efficiency comparison: Accuracy vs. Computational Cost.

| Model | Accuracy (%) Mean ± SD | FLOPS (G) | Efficiency Gain |
|---|---|---|---|
| CNN | 96.60 ± 0.91 | 6.2675 | Baseline |
| EKAN | 95.04 ± 1.05 | 0.2384 | 26.29× |
| FKAN | 96.38 ± 1.13 | 0.2392 | 26.20× |

on different datasets, increasing operational resources (layers/resizing), experimenting with optimization parameters, and testing different one-dimensional functions.

# 5 Conclusions

This study presented a comprehensive evaluation of CNN, EKAN, and FKAN architectures for classifying lung diseases using chest x-ray images, focusing on diagnostic accuracy, convergence stability, and computational efficiency. The quantitative analysis revealed that all evaluated models possess robust predictive capabilities, exceeding 95% in overall average accuracy. While the standard CNN baseline achieved the highest raw accuracy of 96.60%, the FKAN model demonstrated a competitive and statistically comparable performance of 96.38%. Furthermore, the assessment by class highlighted a common diagnostic pattern across all networks. While tuberculosis is easily isolated, as demonstrated by the F1-score evaluation metric, the distinction between normal cases and pneumonia remains a limitation, characterized by a tendency towards false-negative classifications of pneumonia. In this context, FKAN has proven to be the most balanced architecture for reducing these class overlap errors.

Beyond predictive performance, the operational dynamics during the training phase favor the Kolmogorov-Arnold Network (KAN) variants. The baseline CNN exhibited training instability and high loss variance across the cross-validation folds, indicating a vulnerability to local minima and data initialization that could compromise its reliability in clinical deployments without extensive tuning. In contrast, the FKAN model exhibited superior convergence stability. By maintaining the minimal variance and lowest average training loss, at 0.0839, FKAN demonstrated a robust optimization path that solves the training behavior observed in standard convolutional approaches.

Finally, the greatest advantage of the evaluated KAN-based models lies in their remarkable computational efficiency. Both the EKAN and FKAN architectures achieved a significant reduction in memory and processing requirements, requiring more than 26 times fewer operations (GFLOPS) per inference than the baseline CNN. Therefore, the FKAN model stands out as the ideal architecture for this classification task. It successfully preserves the high diagnostic standards of traditional convolutional networks while offering a more stable training process that requires fewer computational resources, making it a highly promising, efficient, and reliable solution for real-world medical applications.

# Declarations

## Authors' Contributions

All authors contributed to the study conception and design. Material preparation, data collection, and implementation were performed by Alexsander Lindolfo de Lima. Analysis was performed by Alexsander Lindolfo de Lima and Jose dos Reis V. Moura Junkior. The first draft of the manuscript was written by Alexsander Lindolfo de Lima and all authors commented on previous versions of the manuscript. All authors read and approved the final manuscript.

## Competing interests

On behalf of all authors, the corresponding author states that there is no conflict of interest.

## Funding

This study was financed in part by the Coordenação de Aperfeiçoamento de Pessoal de Nível Superior – Brasil (CAPES) – Finance Code 001.

## Availability of data and materials

Data used in this study is available for download at https://www.kaggle.com/dsv/10174749 (de Lima [2024]).

# References

Abd Elaziz, M., Fares, I. A., and Aseeri, A. O. (2024). Ckan: Convolutional kolmogorov–arnold networks model for intrusion detection in iot environment. *IEEE Access*. DOI: 10.1109/access.2024.3462297.

Aghaei, A. A. (2025). fkan: Fractional kolmogorov-arnold networks with trainable jacobi basis functions. *Neurocomputing*, page 129414. DOI: 10.1016/j.neucom.2025.129414.

Al-Sheikh, M. H., Al Dandan, O., Al-Shamayleh, A. S., Jalab, H. A., and Ibrahim, R. W. (2023). Multi-class deep learning architecture for classifying lung diseases from chest x-ray and ct images. *Scientific Reports*, 13(1):19373. DOI: 10.1038/s41598-023-46147-3.

Alshmrani, G. M. M., Ni, Q., Jiang, R., Pervaiz, H., and Elshennawy, N. M. (2023). A deep learning architecture for multi-class lung diseases classification using chest x-ray (cxr) images. *Alexandria Engineering Journal*, 64. DOI: 10.1016/j.aej.2022.10.053.

Anthimopoulos, M., Christodoulidis, S., Ebner, L., Christe, A., and Mougiakakou, S. (2016). Lung pattern classification for interstitial lung diseases using a deep convolutional neural network. *IEEE transactions on medical imaging*, 35(5). DOI: 10.1109/tmi.2016.2535865.

Arias-Londoño, J. D., Gómez-García, J. A., Moro-Velázquez, L., and Godino-Llorente, J. I. (2020). Artificial intelligence applied to chest x-ray images for the automatic detection of covid-19. a thoughtful evaluation approach. *Ieee Access*, 8. DOI: 0.1109/access.2020.3044858.

Arsomngern, P., Numcharoenpinij, N., Piriyataravet, J., Teerapan, W., Hinthong, W., and Phunchongharn, P. (2019). Computer-aided diagnosis for lung lesion in companion animals from x-ray images using deep learning techniques. In *2019 IEEE 10th International Conference on Awareness Science and Technology (iCAST)*. IEEE. DOI: 10.1109/icawst.2019.8923126.

Ausawalaithong, W., Thirach, A., Marukatat, S., and Wilaiprasitporn, T. (2018). Automatic lung cancer prediction from chest x-ray images using the deep learning approach. In *2018 11th biomedical engineering international conference (BMEiCON)*. IEEE. DOI: 10.1109/bmeicon.2018.8609997.

Baltruschat, I. M., Steinmeister, L., Ittrich, H., Adam, G., Nickisch, H., Saalbach, A., von Berg, J., Grass, M., and Knopp, T. (2019). When does bone suppression and lung field segmentation improve chest x-ray disease classification? In *2019 IEEE 16th International Symposium on Biomedical Imaging (ISBI 2019)*. IEEE. DOI: 10.1109/isbi.2019.8759510.

Blealtan (2024). Efficient-kan. Available at:`https://github.com/Blealtan/efficient-kan`. GitHub accessed on 12/12/2025.

Bodner, A. D., Tepsich, A. S., Spolski, J. N., and Pourteau, S. (2024). Convolutional kolmogorov-arnold networks. *arXiv preprint arXiv:2406.13155*. DOI: 10.48550/arxiv.2406.13155.

Bozorgasl, Z. and Chen, H. (2024). Wav-kan: Wavelet kolmogorov-arnold networks. *arXiv preprint arXiv:2405.12832*. DOI: 10.2139/ssrn.4835325.

Bresson, R., Nikolentzos, G., Panagopoulos, G., Chatzianastasis, M., Pang, J., and Vazirgiannis, M. (2024). Kagnns: Kolmogorov-arnold networks meet graph learning. *arXiv preprint arXiv:2406.18380*. DOI: 10.48550/arxiv.2406.18380.

Chauhan, A., Chauhan, D., and Rout, C. (2014). Role of gist and phog features in computer-aided diagnosis of tuberculosis without segmentation. *PloS one*, 9(11):e112980. DOI: 10.1371/journal.pone.0112980.

Cheon, M. (2024). Demonstrating the efficacy of kolmogorov-arnold networks in vision tasks. *arXiv preprint arXiv:2406.14916*. DOI: 10.48550/arxiv.2406.14916.

Chokchaithanakul, W., Punyabukkana, P., and Chuangsuwanich, E. (2022). Adaptive image preprocessing and augmentation for tuberculosis screening on out-of-domain chest x-ray dataset. *IEEE Access*, 10. DOI: 10.1109/access.2022.3229591.

De Carlo, G., Mastropietro, A., and Anagnostopoulos, A. (2024). Kolmogorov-arnold graph neural networks. *arXiv preprint arXiv:2406.18354*. DOI: 10.48550/arxiv.2406.18354.

de Lima, A. L. (2024). Raio-x de doenças pulmonares (2º experimento). Accessed on 12/12/2025. DOI: 10.34740/KAGGLE/DSV/10174749.

Drokin, I. (2024). Kolmogorov-arnold convolutions: Design principles and empirical studies. *arXiv preprint arXiv:2407.01092*. DOI: 10.48550/arxiv.2407.01092.

Fatema, K., Mohammed, E. A., and Sehra, S. S. (2025). Taylor-series expanded kolmogorov-arnold network for medical imaging classification. *arXiv preprint arXiv:2509.13687*. DOI: 10.1016/j.mlwa.2026.100929.

Fernández-Miranda, P. M., Fraguela, E. M., de Linera-Alperi, M. Á., Cobo, M., Del Barrio, A. P., González, D. R., Vega, J. A., and Iglesias, L. L. (2024). A retrospective study of deep learning generalization across two centers and multiple models of x-ray devices using covid-19 chest-x rays. *Scientific Reports*, 14(1).

Firsov, N., Myasnikov, E., Lobanov, V., Khabibullin, R., Kazanskiy, N., Khonina, S., Butt, M. A., and Nikonorov, A. (2024). Hyperkan: Kolmogorov–arnold networks make hyperspectral image classifiers smarter. *Sensors (Basel, Switzerland)*, 24(23):7683. DOI: 10.3390/s24237683.

Genet, R. and Inzirillo, H. (2024). Tkan: Temporal kolmogorov-arnold networks. *arXiv preprint arXiv:2405.07344*. DOI: 10.2139/ssrn.4825654.

Gordon, W. J. and Riesenfeld, R. F. (1974). B-spline curves and surfaces. In Barnhill, R. E. and Riesenfeld, R. F., editors, *Computer Aided Geometric Design*, pages 95–126. Academic Press, New York. DOI: 10.1016/b978-0-12-079050-0.50011-4.

Hamal, S., Mishra, B. K., Baldock, R., Sayers, W., Adhikari, T. N., and Gibson, R. M. (2024). A comparative analysis of machine learning algorithms for detecting covid-19 using lung x-ray images. *Decision Analytics Journal*, 11. DOI: 10.1016/j.dajour.2024.100460.

Hasan, M. Z., Montaha, S., Khan, I. U., Hassan, M. M., Al Mahmud, A., Rafid, A. R. H., Azam, S., Karim, A., Prountzos, S., Alexopoulou, E., *et al*. (2024). Fast and efficient lung abnormality identification with explainable ai: A comprehensive framework for chest ct scan and x-ray images. *IEEE Access*, 12. DOI: 10.1109/access.2024.3369900.

He, G., Fu, Y., Cheng, W., Li, Z., Hu, K., Zhang, Y., and Zhu, H. (2026). Vkt: A hybrid vision kan-transformer model for medical image classification. *International Journal of Imaging Systems and Technology*, 36(2):e70334. DOI: 10.1002/ima.70334.

Hornik, K., Stinchcombe, M., and White, H. (1989). Multilayer feedforward networks are universal approximators. *Neural networks*, 2(5). DOI: 10.1016/0893-6080(89)90020-8.

Igali, A. and Shamoi, P. (2024). Image classification using fuzzy pooling in convolutional kolmogorov-arnold networks. In *2024 Joint 13th International Conference on Soft Computing and Intelligent Systems and 25th International Symposium on Advanced Intelligent Systems (SCIS&ISIS)*, pages 1–6. IEEE. DOI: 10.1109/scisisis61014.2024.10760085.

Jiao, L. and Zhao, J. (2019). A survey on the new generation of deep learning in image processing. *Ieee Access*, 7. DOI: 10.1109/access.2019.2956508.

Kermany, D. S., Goldbaum, M., Cai, W., Valentim, C. C., Liang, H., Baxter, S. L., McKeown, A., Yang, G., Wu, X., Yan, F., *et al*. (2018). Identifying medical diagnoses and treatable diseases by image-based deep learning. *cell*, 172(5). DOI: 10.1016/j.cell.2018.02.010.

Kiamari, M., Kiamari, M., and Krishnamachari, B. (2024). Gkan: Graph kolmogorov-arnold networks. *arXiv preprint* *arXiv:2406.06470*. DOI: 10.48550/arxiv.2406.06470.

Kieu, P. N., Tran, H. S., Le, T. H., Le, T., and Nguyen, T. T. (2018). Applying multi-cnns model for detecting abnormal problem on chest x-ray images. In *2018 10th International Conference on Knowledge and Systems Engineering (KSE)*. IEEE. DOI: 10.1109/kse.2018.8573404.

Kiran, S. and Jabeen, D. I. (2024). Dataset of tuberculosis chest x-rays images. Available at:`https://data.mendeley.com/datasets/8j2g3csprk/2`. Accessed on 12/12/2025.

Kolmogorov, A. N. (1957). On the representation of continuous functions of many variables by superposition of continuous functions of one variable and addition. In *Doklady Akademii Nauk*, volume 114. Russian Academy of Sciences. DOI: 10.1090/trans2/028/04.

Lai, R., Williams, T., Rakib, T., Lee, J., and Behar, S. M. (2024). Heterogeneity in lung macrophage control of mycobacterium tuberculosis is modulated by t cells. *Nature Communications*, 15(1). DOI: 10.1038/s41467-024-48515-7.

LeCun, Y., Bottou, L., Bengio, Y., and Haffner, P. (1998). Gradient-based learning applied to document recognition. *Proceedings of the IEEE*, 86(11). DOI: 10.1109/5.726791.

Li, Z. (2024). Kolmogorov-arnold networks are radial basis function networks. *arXiv preprint arXiv:2405.06721*. DOI: 10.48550/arxiv.2405.06721.

Liu, Z., Ma, P., Wang, Y., Matusik, W., and Tegmark, M. (2024a). Kan 2.0: Kolmogorov-arnold networks meet science. *arXiv preprint arXiv:2408.10205*. DOI: 10.48550/arxiv.2408.10205.

Liu, Z., Wang, Y., Vaidya, S., Ruehle, F., Halverson, J., Soljačić, M., Hou, T. Y., and Tegmark, M. (2024b). Kan: Kolmogorov-arnold networks. *arXiv preprint arXiv:2404.19756*. DOI: 10.48550/arxiv.2404.19756.

Muñoz-Aseguinolaza, U., Fernandez-Iriondo, I., Rodríguez-Moreno, I., Aginako, N., and Sierra, B. (2023). Convolutional neural network-based classification and monitoring models for lung cancer detection: 3d perspective approach. *Heliyon*, 9(11). DOI: 10.1016/j.heliyon.2023.e21203.

Pan, W. and Wang, X. (2026). Medvk: Efficient medical image classification via decoupled vision kolmogorov-arnold networks. *Pattern Recognition Letters*. DOI: 10.1016/j.patrec.2026.03.004.

Patel, A. N., Murugan, R., Srivastava, G., Maddikunta, P. K. R., Yenduri, G., Gadekallu, T. R., and Chengoden, R. (2024). An explainable transfer learning framework for multi-classification of lung diseases in chest x-rays. *Alexandria Engineering Journal*, 98. DOI: 10.1016/j.aej.2024.04.072.

Qezelbash-Chamak, J., Hicklin, K., and Kim, M. (2025). Kanbalance: Kolmogorov-arnold network mitigates class imbalance. *Pattern Recognition*, page 112325. DOI: 10.1016/j.patcog.2025.112325.

Rahman, T., Khandakar, A., Kadir, M. A., Islam, K. R., Islam, K. F., Mazhar, R., Hamid, T., Islam, M. T., Kashem, S., Mahbub, Z. B., *et al*. (2020). Reliable tuberculosis detection using chest x-ray with deep learning, segmentation and visualization. *Ieee Access*, 8. DOI: 10.1109/access.2020.3031384.

Riechie, R., Jessica, V., Kurniawan, M., Samosir, F. V. P., *et al*. (2025). Convolutional kolmogorov-arnold network for pneumonia detection in medical image analysis. *Indonesian Journal of Electronics, Electromedical Engineering, and Medical Informatics*, 7(3):475–487. DOI: 10.35882/ijeeemi.v7i3.106.

Somvanshi, S., Javed, S. A., Islam, M. M., Pandit, D., and Das, S. (2024). A survey on kolmogorov-arnold network. *arXiv preprint arXiv:2411.06078*. DOI: 10.1145/3743128.

ul Haque, A., Ghani, S., Saeed, M., and Schloer, H. (2024). Pneumonia classification: A limited data approach for global understanding. *Heliyon*, 10(4). DOI: 10.21203/rs.3.rs-1965784/v1.

Vaca-Rubio, C. J., Blanco, L., Pereira, R., and Caus, M. (2024). Kolmogorov-arnold networks (kans) for time series analysis. *arXiv preprint arXiv:2405.08790*. DOI: 10.1109/gcwkshp64532.2024.11100692.

Wang, G., Zhu, Q., Song, C., Wei, B., and Li, S. (2025). Medkaformer: When kolmogorov-arnold theorem meets vision transformer for medical image representation. *IEEE Journal of Biomedical and Health Informatics*. DOI: 10.1109/jbhi.2025.3541982.

WHO, W. H. O. (2023). The top 10 causes of death. Available at:`https://www.who.int/news-room/fact-sheets/detail/the-top-10-causes-of-death`. Accessed on 12/12/2025.

Xie, X., Lu, Y., Chi, C.-Y., Chen, W., Ai, B., and Niyato, D. (2024). Kansformer for scalable beamforming. *arXiv preprint arXiv:2410.20690*. DOI: 10.1109/tvt.2025.3553860.

Xu, J., Chen, Z., Li, J., Yang, S., Wang, W., Hu, X., and Ngai, E. C.-H. (2024a). Fourierkan-gcf: Fourier kolmogorov-arnold network–an effective and efficient feature transformation for graph collaborative filtering. *arXiv preprint arXiv:2406.01034*. Available at:`https://arxiv.org/html/2406.01034v1`.

Xu, K., Chen, L., and Wang, S. (2024b). Kolmogorov-arnold networks for time series: Bridging predictive power and interpretability. *arXiv preprint arXiv:2406.02496*. DOI: 10.48550/arxiv.2406.02496.

Yang, Z., Zhang, J., Luo, X., Lu, Z., and Shen, L. (2025). Medkan: An advanced kolmogorov-arnold network for medical image classification. *arXiv preprint arXiv:2502.18416*. DOI: 10.1109/bibm66473.2025.11356561.